Extracellular Potassium and Focal Seizures—Insight from In Silico Study

Piotr Suffczynski, Damiano Gentiletti, Vadym Gnatkovsky and Marco de Curtis

Introduction

Epilepsy and seizures have been recognized as brain diseases in antiquity. Since then enormous progress in understanding pathophysiology of epilepsy has taken place. It led to the development of effective treatments, such as antiepileptic drugs [1], resective surgery [2], neuromodulation [3] and neurostimulation [4]. Despite these advances many patients still experience seizures or suffer from side effects of antiepileptic medications. Further progress in understanding mechanisms of epileptic brain activity is needed but the brain complexity at various scales of neuronal organization is the main challenge that needs to be overcome to achieve this goal. There is no existing technology that could possibly measure complex behaviours of thousands of individual neurons synchronizing their electrical activities during seizure. That's why, many properties of neurons, neuronal populations and activities of their networks can be best studied in computational models, where each neuronal element and overall activity may be observed simultaneously. Furthermore, in the case of the brain, a model as complex as the real system would probably be just as hard to investigate. Instead, a wise distinction between essential and irrelevant components of the observed phenomenon may lead to a simplified in silico representation of the complex neuronal system, that may be studied more efficiently. Computational epilepsy research is relatively new but rapidly growing field. Although seizure-like neuronal behaviour has been recreated in a number of

P. Suffczynski (✉) · D. Gentiletti
Department of Biomedical Physics, Institute of Experimental Physics,
University of Warsaw, Pasteura 5, Warsaw, Poland
e-mail: Piotr.Suffczynski@fuw.edu.pl

V. Gnatkovsky · M. de Curtis
Unit of Epileptology and Experimental Neurophysiology,
Fondazione IRCCS Istituto Neurologico Carlo Besta,
Via Giovanni Celoria, 11, Milan, Italy

computational models [5], their applications towards improved clinical practice has been very limited so far. One of the possible reasons is that most of the models of epileptic neuronal networks consider neurons and their connections isolated from the external neuronal environment. Although membrane and synaptic currents are generated by flow of ions across membranes, modelled intra- and extracellular ion concentrations are typically assumed, e.g. in Hodgkin and Huxley formalism [6], to be constant in time and in space. This assumption might hold during normal activity when ion fluxes are moderate and ion homeostasis can be maintained by a number of mechanisms including ion pumps and transporters, buffering and diffusion. However, during periods of increased neuronal discharges, such as seizures, activity-induced changes in ion concentrations may largely deviate from their baseline values [7]. These alterations in intra- and extracellular ion concentrations can impact a number of neuronal processes, such as maintenance of resting membrane potential, operation of voltage-gated channels, synaptic transmission, volume regulation and ion transport mediated by ionic pumps and cotransporters. In particular, extracellular K^+ concentration changes have been directly implicated in epilepsy and seizures [8]. Potassium accumulation hypothesis proposed by Fertziger and Ranck [9] suggests that increased neuronal discharges lead to an increase of extracellular K^+ concentration, which depolarizes neurons leading to their increased firing, what in turn contributes to further increase in extracellular K^+. Such positive feedback mechanism was suggested to be at play during seizures development but also was deemed responsible for seizure termination through depolarization-induced inactivation of Na^+ currents. To date, a lot of experimental data on ion dynamics associated with seizure activity has been accumulated. Nonetheless, these findings are usually not incorporated into computational models, with few notable exceptions (e.g., Durand and Park [10], Kager et al. [11], Krishnan and Bazhenov [12], Wei et al. [13]). These highly realistic models are usually dedicated to particular epilepsy or seizure models. Accordingly, their electrophysiological and ionic patterns might not be similar and it is not yet clear, to what extent these individual results may be generalized.

In this chapter we explore the influence of ionic dynamics on specific seizure generation pattern using computational model with activity-dependent ion concentration changes. The model is based on the experimental data obtained in in vitro isolated guinea pig brain preparation, which is considered an animal model of human focal epilepsy [14]. We show that combined experimental and modelling approach allowed to obtain new insight into functional role played by various ionic components, especially potassium, in focal seizure generation. We also suggest that such better understanding of basic mechanisms underlying epileptic seizures may advance translation of research findings into novel therapeutic applications.

The Scientific Problem

As mentioned above, among four main ions shaping electrical activities of neurons, i.e., Na^+, K^+, Cl^- and Ca^{2+}, dynamics of potassium has been suggested to play an important role in seizure generation. Therefore, we explain the scientific problem by first considering the mechanisms by which extracellular K^+ concentration ($[K^+]_o$) may modulate neuronal excitably. Next, we describe experimentally observed seizure pattern and associated $[K^+]_o$ changes and finally, we formulate the aim of this modelling study.

Effects of Extracellular K^+ Concentration on Neural Activity

Resting Potential

Resting membrane potential is given by the Goldman-Hodgkin-Katz equation (GHK):

$$V_m = \frac{RT}{F} \ln \frac{P_K[K^+]_o + P_{Na}[Na^+]_o + P_{Cl}[Cl^-]_i}{P_K[K^+]_i + P_{Na}[Na^+]_i + P_{Cl}[Cl^-]_o}.$$

For ion concentrations and permeability in typical mammalian cell [15], as shown in Table 1, the resting membrane potential is −66 mV.

Figure 1 shows the influence of concentrations of K^+, Na^+ and Cl^- on resting membrane potential, calculated according to GHK equation. On each graph, variation of the resting membrane potential is shown (solid line) when given concentration is being varied and all others are kept constant, at their baseline values. The reference value of a concentration being varied is shown on each graph by broken vertical line. Intersection of solid and broken lines on each graph marks the reference resting membrane potential, that is $V_m = -66$ mV. The slope of the solid line on each graph corresponds to sensitivity of the resting membrane potential to changes of the given concentration. One can see that resting membrane potential depends on all concentrations but it is most sensitive to change of extracellular potassium, as suggested by largest slope of the solid line in Fig. 1 left bottom panel, as compared to other panels. It suggests that even moderate increase of $[K^+]_o$ leads to significant change of the resting potential of the cell into depolarized direction.

Table 1 Ion concentrations in a typical mammalian cell

Ion	Inside (mM)	Outside (mM)
K^+	140	5
Na^+	10	145
Cl^-	4	110
Ca^{2+}	$1 * 10^{-4}$	2.5

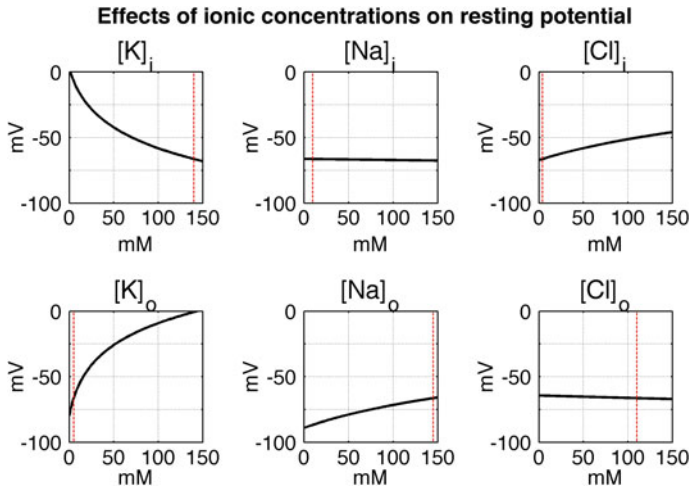**Effects of ionic concentrations on resting potential**

Fig. 1 Influence of K$^+$, Na$^+$ and Cl$^-$ concentration changes on the resting membrane potential. On each graph, *black solid line* shows the resting membrane potential calculated with GHK equation while *red vertical broken line* shows the reference value of the given concentration. Crossing of these lines marks the resting membrane potential for the reference conditions, that is about −66 mV. The resting membrane potential is sensitive to changes of all concentrations but it most sensitive to change of potassium extracellular concentration. Even minor change of extracellular K$^+$ concentration around its reference value leads to significant change of the resting membrane potential

Driving Force

The main role of all potassium currents is to control excitability and stabilize membrane potential around potassium reversal potential E_K, typically around −90 mV. Ionic current is proportional to the channel conductance and the ionic driving force, which is the difference between the membrane potential and the ion reversal potential. The ionic reversal potential in turn depends on the intra- and extracellular ion concentrations. When extracellular potassium increases, both potassium reversal potential and the resting membrane potential move to more positive level. However, E_K grows more considerably than membrane potential V_m, because change of V_m is limited by the presence of Na$^+$ and Cl$^-$ leak currents. As a result, E_K moves towards V_m leading to reduction of the driving force of all potassium currents. Accordingly, the cell's capability to resist membrane depolarization is diminished and may lead to increased action potential firing.

Synaptic Transmission

Effect of extracellular potassium on synaptic transmission is not trivial as both pre- and postsynaptic part of the synapse depend on membrane depolarization and therefore on $[K^+]_o/[K^+]_i$. It is established experimentally [16] that moderate increase of $[K^+]_o$ enhances excitatory synaptic transmission while above certain level of $[K^+]_o$ both excitatory and inhibitory synaptic transmission is abolished due to presynaptic depolarization-related inactivation of Na^+ and Ca^{2+} channels. Yet another effect is related to interaction between potassium and chloride. $GABA_A$ inhibitory potentials are associated with chloride influx that hyperpolarizes the cell. The Cl^- and K^+ ions are coupled by potassium-chloride co-transporter KCC2, which usually extrudes K^+ and Cl^- ions from neurons [17]. The KCC2 co-transporter operates at thermodynamic equilibrium defined by $[K^+]_o[Cl^-]_o = [K^+]_i[Cl^-]_i$ [18]. Under this condition, large increase of extracellular K^+ concentration must be compensated by increase of intracellular Cl^- and the direction of transport of K^+ and Cl^- ions reverses. It leads to intracellular Cl^- accumulation and elevation of the $GABA_A$ reversal potential. Accordingly, $GABA_A$ inhibitory potentials will be reduced or may even become depolarizing if E_{GABAA} surpasses membrane potential of the cell [19].

Focal Seizure Dynamics

Many types of epileptic seizures are not stationary processes but exhibit intrinsic dynamics. From the clinical point of view, seizure onset patterns are most important, as they are relevant for seizure early detection and localisation. However, seizure evolution may provide important clues regarding the mechanism involved in seizure generation. The typical pattern observed with intracranial electrodes in mesial temporal lobe epilepsy patients consists of low-voltage fast activity (>25 Hz) at the seizure onset, irregular activity phase with some increase of amplitude followed by synchronous quasi-rhythmic pattern that increases in spatial synchrony towards the end of the seizure. These focal seizure patterns can be reproduced and studied in animal in vitro models, which offer an additional advantage of performing intracellular and ion-selective recordings together with extracellular LFP measurements in the intact, whole brain networks.

In in vitro isolated guinea pig brain preparations [20] seizures may be induced acutely by arterial application of proconvulsant drugs [21]. Seizure patterns in this model resemble very much those observed in human focal epilepsy [14]. Intracellular recordings from entorhinal cortex (EC) neurons showed that seizures were initiated with increased firing of inhibitory interneurons and neuronal silence of principal cells, which correlated with low-voltage fast LFP oscillations (20–30 Hz). Neuronal firing of principal cells was subsequently restored with an acceleration-deceleration firing pattern followed by rhythmic burst activity. Increased firing of principal neurons correlated with ictal discharges in the LFP signal. An increase of

extracellular potassium concentration was observed throughout the seizure. Typical intracellular seizure pattern and associated extracellular potassium concentration time course observed in isolated guinea pig brain is shown in Fig. 3a.

Aim of This Work

Despite the fact that the synaptic and non-synaptic mechanisms mediating seizure pattern observed in isolated guinea pig brain have been suggested, the specific roles played by various neural elements during seizures are not fully understood. During seizure states many mechanisms are interacting in complex ways, making it difficult to study experimentally. It is becoming recognized that studying these interactions may contribute to a better understanding of seizure generation. The aim of the present chapter is to investigate the link between ionic dynamics and experimentally observed seizure pattern, using a computational model, in order to provide such a synthetic view.

Computational Methods

Model Description

The model consists of two multicompartmental EC cells, a pyramidal neuron and an inhibitory interneuron, embedded in the common extracellular space (ECS) surrounded by a bath. The size of ECS was estimated by the extracellular volume fraction α defined by the ratio volume of extracellular space/volume of intracellular space. Ionic dynamics of K^+, Na^+, Ca^{2+} and Cl^- was incorporated and activity-dependent changes in their concentrations were computed. Concentration changes in a given extra- or intracellular compartment were dependent on a number of mechanisms such as: active and passive membrane currents, inhibitory synaptic $GABA_A$ currents, Na^+/K^+ pump, KCC2 cotransporter, glial K^+ buffering, radial diffusion between ECS and bath, and longitudinal diffusion between dendritic and somatic compartments. At each simulation step all ionic concentrations were updated and their reversal potentials were computed. The model setup is shown in Fig. 2. Simulations were performed using NEURON simulator with a fixed integration step of 0.05 ms. The parameters' values and units together with their sources are given in Gentiletti et al. [22]. Modifications in the present model, with respect to original publication include: (i) simplified cells' morphology, (ii) leak currents for K^+, Na^+, and Cl^- (instead of K^+, Na^+ and fixed leak), (iii) modification of radial diffusion coefficients to better reproduce experimental results, (iv) taking into account bicarbonate and Cl^- concentrations for calculation of E_{GABAA} (instead of considering only Cl^-). These changes are described in the subsequent sections, where modified parameter values are provided.
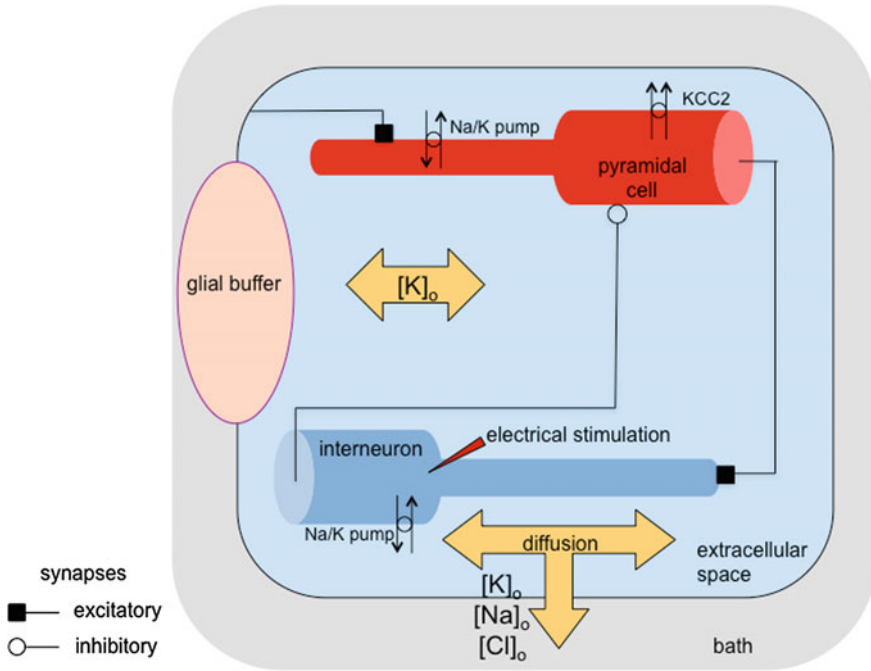
Fig. 2 Schematic diagram of the model. Two entorhinal cortex cells, a pyramidal cell and an interneuron are synaptically coupled and are embedded in the common extracellular space, which is surrounded by a bath. The model includes ionic regulation mechanisms: Na^+/K^+ pump in both cells, KCC2 cotransporter in pyramidal cell, glial buffering of K^+ ions and diffusion of K^+, Na^+ and Cl^- ions between compartments and between extracellular space and surrounding bath. The activity in the model can be triggered by excitatory synaptic input to pyramidal cell and current input to the interneuron

Cells' Morphology

The cells in our model were adapted from the compartmental model of the EC cells by Fransén et al. [23]. In the original model the pyramidal cell was composed of six compartments, one representing the soma, three representing the apical dendrite and two representing basal dendrites. The interneuron was composed of six compartments, one representing the soma, three representing a principal dendrite, and two representing remaining dendrites. In order to simplify the given models we lumped together all dendrites in both cells using Rall's rule. Therefore, the simplified model of pyramidal cell is composed of two compartments: one representing soma with length 20 μm and diameter 15 μm, and one representing lumped dendrites with length 450 μm and diameter 6.88 μm. The interneuron is also composed of two compartments, one representing soma with length 20 μm and diameter 15 μm and one representing lumped dendrites with length 700 μm and diameter 3 μm. The extracellular space is common for both cells, but is physically modelled around the

interneuron. It consists of two cylindrical compartments, one surrounding the soma and one surrounding the dendrite. Each extracellular compartment communicates with the corresponding intracellular compartment of the modelled neurons, neighbouring extracellular compartment, glial buffer and bath. To account for the fact that each extracellular compartment corresponds to common ECS of pyramidal cell and interneuron and that each cell contributes roughly similar extracellular volume, the volume of each common extracellular compartment is given by twice the volume of the corresponding extracellular compartment of the interneuron.

Cells' Biophysics

Reversal Potentials and Passive Electrical Properties

The reversal potential of the ions is given by Nernst equation:

$$E_X = \frac{RT}{zF} \ln\left(\frac{[X]_o}{[X]_i}\right)$$

where $[X]_i$ and $[X]_o$ represent intra and extracellular concentrations, respectively of the ionic species $X = \{Na^+, K^+, Ca^{2+}, Cl^-\}$, F is Faraday's constant, R is the gas constant, z is the valence of the species X and $T = 32\ °C$ is temperature (as specified in Gnatkovsky et al. [24]). Leakage currents were present in all the compartments of both cells and had the following, standard expressions:

$$I_{Na, leak} = g_{Na, leak}(V_m - E_{Na})$$
$$I_{K, leak} = g_{K, leak}(V_m - E_K)$$
$$I_{Cl, leak} = g_{Cl, leak}(V_m - E_{Cl})$$

The resting membrane potential was set to −65 mV in the pyramidal cell and −75 mV in the interneuron. In pyramidal cell we set initial potassium and chloride concentrations at the thermodynamic equilibrium of KCC2, i.e., $[K^+]_o[Cl^-]_o = [K^+]_i[Cl^-]_i$. In this way, potassium and chloride cotransporter currents were zero initially and membrane potential was more stable. Specific axial resistance in both cells was set to $R_a = 100$ Ohm $\times$ cm and specific membrane capacitance was set to $C_m = 1 \mu F/cm^2$, as in Fransén et al. [23]. It should be noted that under background excitatory synaptic input, ionic concentrations and membrane potentials deviated slightly from the equilibrium conditions.

Active Currents

The pyramidal cell model included the following active membrane currents: the Na$^+$ and K$^+$ currents present in both compartments and responsible for fast action potentials (I_{NaT} and I_{Kdr}, respectively); a persistent Na$^+$ current I_{NaP} in the soma; a high-threshold Ca^{2+} current I_{CaL} in both compartments; a calcium-dependent K$^+$ current I_{KAHP} in both compartments; a fast calcium- and voltage-dependent K$^+$ current I_{KC} in both compartments; and a noninactivating muscarinic K$^+$ current I_{KM} in the soma. The interneuron model had the Na$^+$ and K$^+$ currents, I_{NaT} and I_{Kdr}, in both compartments, responsible for fast action potentials. All the models of active currents were based on Fransén et al. [23]. Some changes of the parameters were required in order to compensate the additional ionic regulation mechanisms that were not present in the original model. Implemented modifications together with all the currents' formulas and parameters are given in Gentiletti et al. [22].

Synaptic Connections and Network Inputs

The pyramidal cell and inhibitory interneuron are synaptically coupled, as shown in Fig. 2. An inhibitory synapse is placed in the middle of somatic compartment of the pyramidal cell, and an excitatory synapse is placed in the middle of dendritic compartment of the interneuron. The synaptic conductances are modelled according to NEURON's built-in Exp2Syn mechanism with a double-exponential function of the form:

$$g = g_{\max}[\exp(-t/\tau_2) - \exp(-t/\tau_1)]$$

The τ_1 and τ_2 are the rise and decay time constants respectively, taking values 2 ms and 6 ms for all synapses. The reversal potential of excitatory postsynaptic currents (EPSC) was set to 0 mV. In order to investigate the impact of chloride concentration changes the inhibitory GABA$_A$ postsynaptic currents were explicitly mediated by chloride influx. Because GABA$_A$ receptor pore conducts both Cl$^-$ and HCO$_3^-$ in a 4:1 ratio [25], E_{GABAA} was calculated using the Goldman-Hodgkin-Katz equation [26]:

$$E_{GABAA} = \frac{RT}{F} \ln\left(\frac{4[Cl^-]_i + [HCO_3^-]_i}{4[Cl^-]_o + [HCO_3^-]_o}\right)$$

For simplicity, HCO$_3^-$ concentrations were assumed to be constant and equal to [HCO$_3^-$]$_i$ = 15 mM and [HCO$_3^-$]$_o$ = 25 mM. Excitatory and inhibitory synaptic weights w_e, w_i were equal to 0.001 and 0.002 μS, respectively. With these settings, the unitary excitatory postsynaptic potential had amplitude of $\sim$2.3 mV at the soma, while the unitary inhibitory postsynaptic potential had amplitude of $\sim$1 mV at the soma. A synaptic response was generated in a postsynaptic cell when presynaptic membrane potential in the soma crossed the threshold of −10 mV.

Pyramidal cell received excitatory background synaptic input via dendritic excitatory synapse activated by a Poisson spike train with 66 Hz rate. In order to reproduce enhanced interneuronal firing at seizure onset, the inhibitory interneuron was stimulated by the somatic injection of a depolarizing current with initial amplitude of 1.3 nA at second 13 that was linearly decreasing toward 0.5 nA at second 60.

Ion Accumulation

Changes in ion concentrations due to transmembrane currents are described by the following equation:

$$\frac{d[X]}{dt} = \frac{\sum I_X}{zFV},$$

where $[X]$ is the concentration of the ionic species X, ΣI_X is the net ion transmembrane current, F is Faraday's constant, V the compartment volume, and z the valence of the species X. The right-hand side is positive if the net flow is outward (for positive z), negative, if inward. The longitudinal diffusion contribution is calculated using the built-in mechanism in the NEURON simulation environment:

$$\frac{d[X_i]}{dt} = D_X \sum_n \frac{([X_j] - [X_i])S_{ij}}{L_{ij}V_i},$$

where $[X_i]$ is the ion concentration in the compartment i, D_X is the longitudinal diffusion constant of the ionic species X, S_{ij} is the flux area between the adjacent compartments i and j, L_{ij} is the distance between the centers of the compartments i and j, and V_i is the volume of the compartment i. The right-hand side is positive if the net flow is increasing the ion concentration of the given compartment, negative otherwise. The sum is made over the total number of contributions to ionic concentration in the i-th compartment. For our two compartmental cells and ECS n is equal to 1. The ions accumulated in the extracellular space can diffuse radially to the bath representing the extracellular space and vasculature not included in the model. Radial diffusion represents the net effect of various processes such as extracellular diffusion to more distant areas of the brain, potassium transport into capillaries and potassium regulation by the network of glial cells coupled by gap junctions. The time constant of these joint processes is likely to be much slower than that of lateral diffusion. Therefore radial diffusion constant is assumed to be equal to the longitudinal diffusion constant D_X, divided by a scale constant $s = 5000$. Bath concentrations are assumed to be constant and equal to the initial extracellular concentrations. For the sake of simplicity, radial ion diffusion was modelled only for K^+, Na^+ and Cl^-, as Ca^{2+} fluxes were much smaller than these of other ion types. The equation implemented to account for radial diffusion is as follows:

$$\frac{d[X_i]_o}{dt} = \frac{1}{s} D_X \frac{([X]_{bath} - [X_i]_o)S_i}{(dr/2)V_i},$$

where $[X]_{bath}$ is ion X concentration in the bath, S_i is radial flux area corresponding to the i-th compartment, V_i is the volume of the i-th extracellular compartment, and dr is the thickness of the extracellular space. The values of radial diffusion constants (in $[\mu m^2/ms]$) for K^+, Na^+ and Cl^- were 1.96, 0.226 and 2.03, respectively. The electrostatic drift of ions was neglected, as the ion movement due electrical potential gradient in extracellular space is small compared to diffusion.

Na^+/K^+ Pump

The Na^+/K^+ pump is moving Na^+ and K^+ ions across the membrane in order to maintain their concentration gradients and exchanges 2 K^+ ions for 3 Na^+ ions. The Na^+ and K^+ pump currents are as is [27]:

$$I_{Na} = 3I_{max} flux([Na^+]_i, [K^+]_o)$$
$$I_K = 2I_{max} flux([Na^+]_i, [K^+]_o)$$
$$flux([Na^+]_i, [K^+]_o) = \left(1 + \frac{Km_K}{[K^+]_o}\right)^{-2} \left(1 + \frac{Km_{Na}}{[Na^+]_i}\right)^{-3}$$

using maximal flux $I_{max} = 0.0013$ mA/cm^2, $Km_K = 2$ mM and $Km_{Na} = 10$ mM.

Glial Buffer

Potassium buffering is modelled with a first-order reaction scheme simulating glial potassium uptake system. It involves three variables: $[K^+]_o$—extracellular potassium concentration, $[B]$—free buffer, $[KB]$—bound buffer, and backward and forward rate constants k_1 and k_2, respectively. The set of differential equations solved is as follows [27]:

$$\frac{d[K^+]_o}{dt} = -k_2[K^+]_o[B] + k_1[KB]$$
$$\frac{d[B]}{dt} = -k_2[K^+]_o[B] + k_1[KB]$$
$$\frac{d[KB]}{dt} = -k_2[K^+]_o[B] - k_1[KB]$$

KCC2 Cotransporter

In adult hippocampal cells low intracellular Cl^- concentration is maintained by means of potassium-chloride cotransporter KCC2 that mediates $K - Cl$ cotransport across the membrane. The transport process involves one for one extrusion of Cl^- ion together with K^+ ion. The KCC2 cotransporter currents are modelled according to Wei et al. [13]:

$$I_K = \gamma U_{KCC2} \ln\left(\frac{[K^+]_i [Cl^-]_i}{[K^+]_o [Cl^-]_o}\right)$$

$$I_{Cl} = -I_K$$

where $U_{KCC2} = 0.3$ mM/s is the cotransporter strength and $\gamma = S_i/(FV_i)$ is a conversion factor from the concentration per second units (mM/s) to the current density units (mA/cm^2). For pyramidal compartments, soma and dendrite, γ takes the value γ_s and γ_d, respectively. The parameters S_i, V_i, are the total surface area and total intracellular volume of the respective cell compartment and F is Faraday's constant.

Results

In Silico Test of the Whole Brain In Vitro Hypothesis

Experimental studies of seizures in the entorhinal cortex of the in vitro isolated guinea pig brain [14, 24] showed that onset of ictal episodes is associated with strong discharge of inhibitory interneurons and initial silence of principal cells, which are subsequently recruited into progressively synchronized discharges. It was proposed that interneuronal firing-related increase of extracellular potassium together with intracellular chloride accumulation and reduction of GABA$_A$ inhibition results in hyperexcitability of principal cells and progression of a seizure. We tested this hypothesis using our computational model. A comparison of experimental and modelling results is shown in Fig. 3. In the model the seizure-like event was initiated by depolarizing current applied to soma of the inhibitory interneuron as shown by red trace in Fig. 3b middle panel. Current stimulation triggered strong interneuronal discharge at the initial rate of about 300 Hz. The membrane potential of the pyramidal cell transiently decreased and the cell ceased firing following onset of strong inhibitory drive (considered as the beginning of the seizure). After gap in firing lasting about 7 s, pyramidal cell resumed its activity reaching maximal firing rate of about 8 Hz in about 11 s from seizure onset. Throughout the seizure, inhibitory interneuron exhibited tonic discharges with gradually decreasing spike amplitude. These changes were accompanied by increase of extracellular potassium concentration, which increased sharply, reached maximal value of 9 mM within first seconds of the seizure and slightly decreased afterwards. These simulation
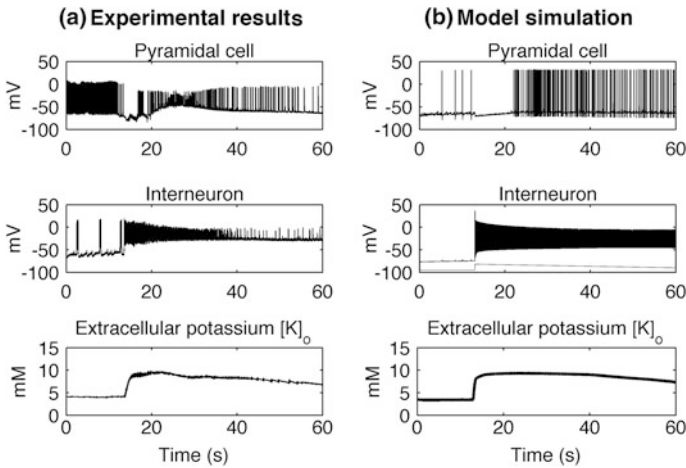
Fig. 3 Comparison between experimental data (**a**) and model simulation (**b**), Experimental recordings obtained in entorhinal cortex of in vitro isolated guinea pig brain show intracellular traces of pyramidal cell (*top panel*), interneuron (*middle panel*) and extracellular potassium (*bottom panel*). Seizure onset is associated with increased firing of the inhibitory interneuron and cessation of firing in pyramidal cell for few seconds. Afterwards, principal cell resumes its tonic activity that progressively transforms into bursts. Extracellular potassium is elevated up to 9 mM within first few seconds of the seizure and remains elevated throughout the seizure. Activity patterns of both cells (except bursting) and extracellular potassium time course are reproduced by the model. In the model discharge of the interneuron is triggered by somatic injection of the depolarizing current, shown in *red* in part (**b**), *middle panel*

results agree qualitatively and quantitatively in many respects with the experimentally observed seizures in the isolated guinea pig brain (Fig. 3a). To make the role of inhibitory interneurons more evident the pyramidal cell shown in Fig. 3a was stimulated by a steady positive current delivered via the intracellular pipette. The resulting depolarization was responsible for fast discharge present before the seizure. Initial discharge of interneurons at a rate about 400 Hz transiently inhibited pyramidal cells, which stopped firing but resumed their activity within few seconds, reached maximal firing rate of 9 Hz about 13 s from seizure onset and gradually decreased afterwards. Strong firing of the interneuron gradually decreased and exhibited reduction of spike amplitude. Extracellular potassium concentration attained its maximal value of 9.5 mM few seconds after seizure onset and slowly decreased subsequently.

End of the seizure, characterized by bursting firing pattern of pyramidal cells, is not yet captured by the model. If the simulation is prolonged beyond second 60, the interneuron enters depolarization block (around second 80) and pyramidal cells exhibits slow and steady decrease of the firing rate, reaching initial background firing rate around second 120.

Relationship Between Intracellular Seizure Patterns and Ion Concentration Changes

The distinctive firing patterns observed in the model during seizure-like events result from the interplay between synaptic mechanisms, membrane currents and ion concentration changes. Summary of changes of concentration gradients and corresponding reversal potentials of K^+, Na^+ and Cl^- is shown in Fig. 4. Seizure onset is associated with fast rise of extracellular potassium concentration and increase of potassium reversal potentials in both interneuron and pyramidal cell (Fig. 4a, b, first column). Initially pyramidal cell is inhibited by strong GABA$_A$ receptor-mediated currents and ceases firing. Slowing down of interneuron discharge and intracellular chloride accumulation in pyramidal cell (Fig. 4a, third column) both contribute to reduction of IPSPs and increase of membrane potential of pyramidal cell. Additionally, amplitude of action potentials generated by the interneuron gradually declines due to decrease of sodium reversal potential (Fig. 4b, second column). When the spike amplitude in the interneuron falls below -10 mV the inhibitory synaptic transmission is prevented. An increase of extracellular potassium
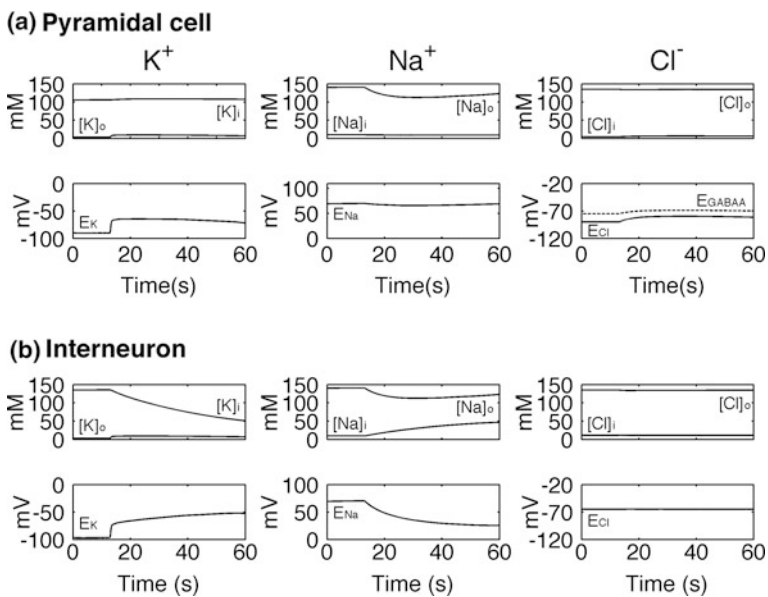

Fig. 4 Summary of changes of ionic activities in pyramidal cell (**a**) and interneuron (**b**) during modelled seizure episodes. For each cell and ion type, intra- and extracellular concentrations are shown in upper panel and reversal potentials are shown in bottom panel. Seizure-like activity is associated with significant ion concentration changes in both cells. Accordingly, in pyramidal cell potassium, chloride and GABAA reversal potentials are elevated, while that of sodium is reduced. In interneuron potassium reversal potential increases while sodium potassium reversal exhibits markedly declines

concentration together with loss of inhibition causes pyramidal cell to resume its activity within few seconds from seizure onset. Initially strong pyramidal cell discharge slows down as a result of slow decrease of extracellular potassium leading to decrease of potassium reversal potential and associated increase of outward potassium leak current.

Neuronal $[K^+]_o$ Sources and Regulation

The dynamic increase of extracellular potassium concentration seems to be a primary factor leading to development of seizure-like events in the model. Accordingly, we investigated the sources of $[K^+]_o$ accumulation in pyramidal cell and interneuron. To this end, we computed time integral of various potassium membrane currents and divided the result by the volume of the corresponding extracellular space. The contributions of $[K^+]_o$ from the interneuron soma are shown in Fig. 5, while those from the pyramidal cell soma are shown in Fig. 6. One can notice that the dominant $[K^+]_o$ contribution comes from action potential firing in the interneuron (Fig. 5, upper panel, red diamonds), while contribution from potassium leak current in the interneuron is negligible (Fig. 5, upper panel, blue circles). Potassium current due to Na^+/K^+ pump contributes to $[K^+]_o$ removal (Fig. 5, upper panel, green stars), but cannot balance potassium outflow and the net result is positive (Fig. 5, lower panel). In the pyramidal cell, contributions from leak and all voltage-gated potassium membrane currents are negligible. The dominant influence comes from KCC2 cotransporter, which due to high $[K^+]_o$ conditions, lowers $[K^+]_o$
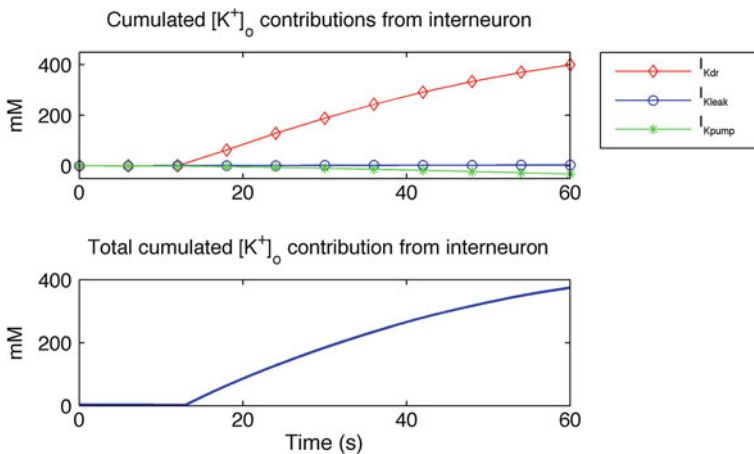

Fig. 5 *Upper panel* cumulated potassium fluxes in the interneuron. The largest outward flux corresponds to I_{Kdr} current (*red diamonds*), while the inward flux is mediated by potassium current generated by the Na^+/K^+ pump (*green stars*). *Lower panel* total accumulated potassium in extracellular space due to potassium fluxes in the interneuron
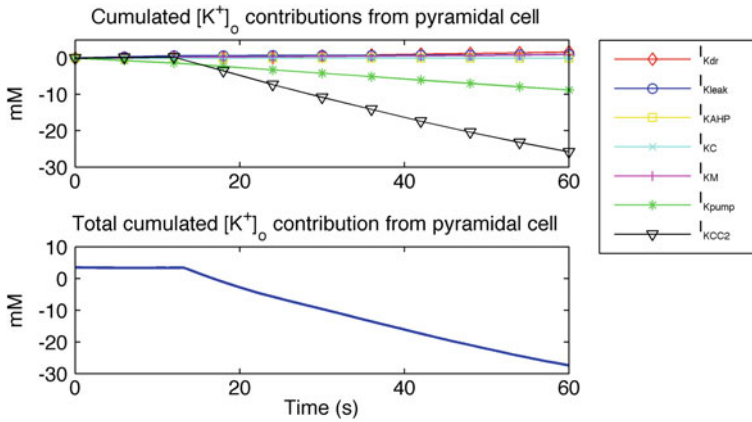
Fig. 6 *Upper panel* cumulated potassium fluxes in the pyramidal cell. The outward fluxes mediated by potassium membrane currents are negligible. The inward fluxes are mediated by potassium current generated by the Na^+/K^+ pump (*green stars*) and KCC2 (*black triangles*). Lower panel: total cumulated potassium is negative, what means that potassium is up-taken from extracellular space by pyramidal cell

by cotransport of K^+ and Cl^- ions into the cell (Fig. 6, upper panel, black triangles). The transport of K^+ by Na^+/K^+ pump in pyramidal cell is inward and reduces $[K^+]_o$ as in interneuron (Fig. 6, upper panel, green stars). Because in pyramidal cell potassium inward flux is of larger magnitude than the outward flux the net amount of $[K^+]_o$ regulated by that cell is negative (Fig. 6, lower panel).

The $[K^+]_o$ Balance

Apart from membrane contributions and regulation of $[K^+]_o$, potassium accumulation is additionally regulated by a glial uptake, lateral diffusion to neighbouring compartment and radial diffusion to the bath. The net effect of membrane currents and these additional mechanisms is responsible for time course of $[K^+]_o$ observed during model activity. The individual components shaping $[K^+]_o$ time course in the somatic extracellular compartment are shown in Fig. 7 (upper panel), while the resulting extracellular potassium balance is shown in Fig. 7 (lower panel). This trace is equivalent to that shown in Fig. 3b (lower panel). The dominant contribution to $[K^+]_o$ comes from the interneuron (Fig. 7, upper panel, red diamonds). Extracellular potassium clearance is mediated by uptake by glia and pyramidal cell and by lateral and radial diffusion. Initially glial uptake (Fig. 7, upper panel, green stars) plays a dominant role but as $[K^+]_o$ builds up and remains elevated, diffusion processes (Fig. 7, upper panel, pink circles and black crosses) become main mechanisms of potassium regulation. Despite both the inward and outward flows of potassium produce cumulated extracellular concentrations of the order of hundreds
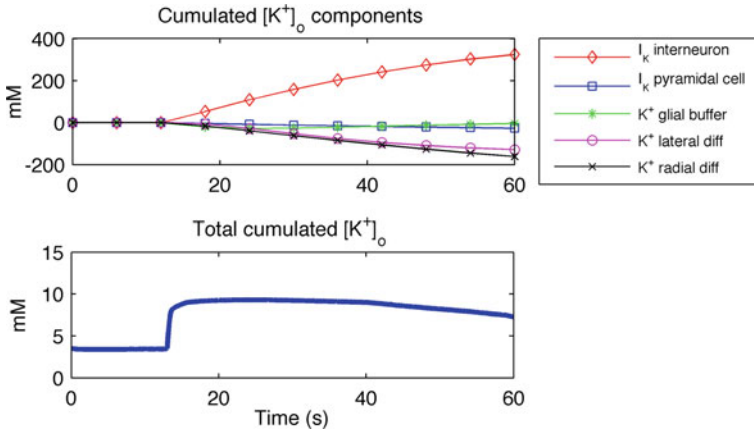
Fig. 7 *Upper panel* cumulated potassium fluxes mediated by the pyramidal cell, interneuron, glial buffer and diffusion. The outward flux is mediated by potassium action potential currents in the interneuron (*red diamonds*). Potassium clearance is mediated initially by glial buffer (*green stars*) and subsequently by lateral- and radial diffusion (magenta circles and *black crosses*). *Lower panel* total cumulated potassium due to all potassium fluxes in the model

of mM, the total cumulated extracellular potassium is of the order of 10 mM, showing that the processes of potassium release and clearance operate at a fine balance.

Selective Impairment of Potassium Homeostasis Mechanisms

To investigate the effects of various components of potassium homeostasis implemented in the model, the potassium clearance mechanisms were selectively removed and simulations of such altered models were performed. These hypothetical manipulations show how impairment of a certain neuronal process may affect behaviour of cells and extracellular potassium.

When the glial buffer was removed, $[K^+]_o$ increased rapidly up to around 25 mM causing depolarization block in pyramidal cell during the whole simulation (Fig. 8, top trace). Interneuron continued to fire but within few seconds spike amplitude was severely reduced (Fig. 8, middle trace), limiting further release of potassium. Consequently $[K^+]_o$ started to decrease due to clearance by Na^+/K^+ pump and diffusion (both lateral and radial), reaching a final value of ~10 mM.

The effect of removal of potassium diffusion in the model is shown in Fig. 9. In this case, $[K^+]_o$ increased rapidly up to around 10 mM causing depolarization block in pyramidal cell during the whole simulation (Fig. 9, top trace). Interneuron fired with gradually decreasing spike amplitude until second 40 and entered depolarization block afterwards (Fig. 9, middle trace). $[K^+]_o$ was increasing throughout the simulation showing limited ability of glial buffer and Na^+/K^+ pump to clear

Fig. 8 Model simulations with removed glial uptake mechanisms. Soon after seizure onset $[K^+]_o$ attains high value of about 25 mM and pyramidal cell enters permanent depolarization block. Interneuronal activity is maintained but with drastically reduced spike amplitude
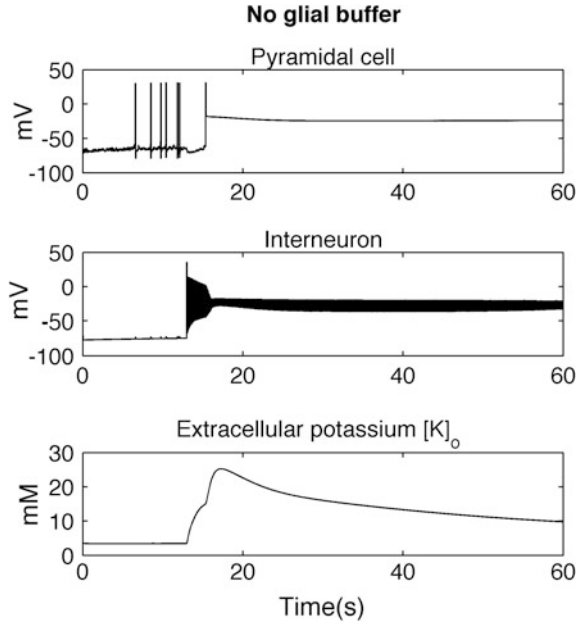
potassium effectively (Fig. 9, bottom trace). When glial buffer was filled-up around second 40, $[K^+]_o$ rose to the level of around 25 mM causing depolarization block of the interneuron.

Finally, Fig. 10 shows the model behaviour in the absence of the Na^+/K^+ pump. Absence of the pump caused abnormal firing of the pyramidal cell (Fig. 10, top trace), associated with small build-up of $[K^+]_o$ even before the application of the depolarizing current to the interneuron (Fig. 10, bottom trace). When interneuron started to fire, $[K^+]_o$ rose sharply to a value above 10 mM causing depolarization block in pyramidal cell. Interneuron fired with gradually decreasing spike amplitude until second 45 and entered depolarization block afterwards (Fig. 10, middle trace). The overall time course of $[K^+]_o$ was similar to that obtained for the reference conditions but $[K^+]_o$ levels were slightly higher. Here $[K^+]_o$ reached maximal and final value of $\sim$10.5 mM and $\sim$7.5 mM, respectively (vs. $\sim$9.3 mM and $\sim$7.2 mM for the intact model).

In summary, removal of any of the potassium regulatory mechanisms had significant effect on the model dynamics. Blocking of the diffusion process or glial buffering system led to depolarization block of pyramidal cell and high extracellular potassium reaching concentration above 25 mM, what may correspond to spreading depression episode. Impairment of the Na^+/K^+ pump led to depolarization block of both cells but extracellular potassium concentration was similar to that in the intact model. It shows that in the model, diffusion process and glial buffering is more effective in potassium clearance that the Na^+/K^+ pump. This result is in agreement with earlier observations of relative role of potassium regulatory mechanisms, illustrated in Fig. 7.

Fig. 9 Model simulations with removed diffusion mechanisms. Soon after seizure onset pyramidal cell enters permanent depolarization block. $[K^+]_o$ gradually increases and reaches maximal value about 25 mM around second 40. Interneuron exhibits firing with decreasing spike amplitude for about 30 s and enters depolarization block afterwards
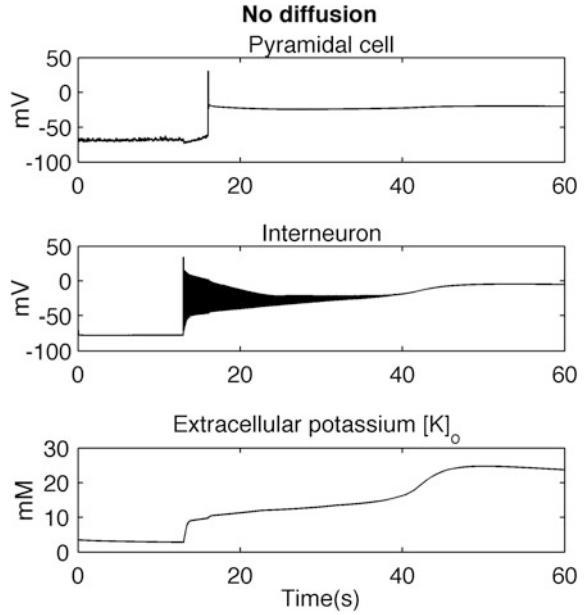
Fig. 10 Model simulations with removed Na^+/K^+ pump. Absence of the pump causes slight intial increase of $[K^+]_o$ and associated strong firing of pyramidal cell. Soon after seizure onset pyramidal cell enters permanent depolarization block, similar to one observed in Figs. 8 and 9. Interneuron enters depolarization block around second 45, while extracellular potassium time course is similar and only slightly elevated as compared to simulation of the intact model
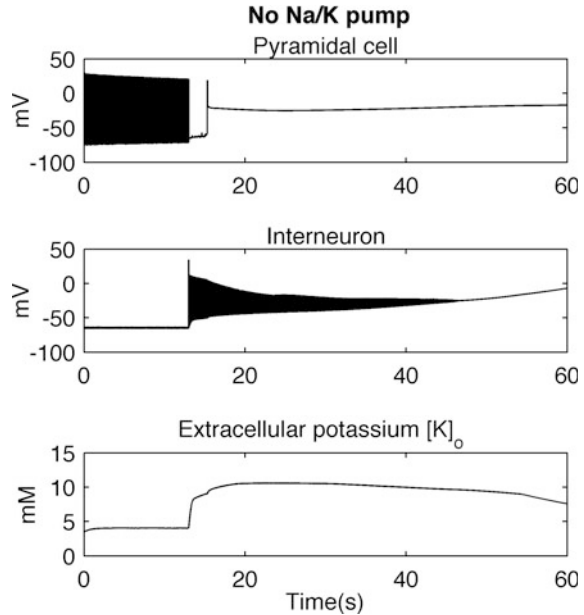
Future Therapies

Currently 38% of newly diagnosed adult patients with localisation related epilepsy are drug resistant [28]. This number remains almost unchanged since the discovery of the first modern antiepileptic drug over hundred years ago [29]. It shows that new concepts and investigation of other therapeutic strategies is necessary. Using the model we investigated whether introduction of artificial extracellular potassium regulation mechanism might successfully control neuronal excitability. Potassium regulation was implemented as additional potassium buffer with the activation threshold 3.5 mM and buffering speed 0.8 mM/ms. Such a mechanism could be possibly realized in practice by a nanoparticle system as innovative applications of nanomaterials in medicine continue to emerge [30]. Model simulations with nanoparticle buffering agent present in the extracellular space are shown in Fig. 11. Strong interneuronal firing (Fig. 11, middle trace) that would normally cause increase of extracellular potassium and abnormal pyramidal cell discharges was ineffective in triggering seizure-like episode in the presence of the artificial buffer. Potassium remained at its baseline level (Fig. 11, bottom trace) and when inhibition decreased following $[Cl^-]_i$ accumulation, pyramidal cell resumed normal activity (Fig. 11, top trace). It shows that such artificial $[K^+]_o$ regulation mechanism might lead to successful seizure control.

Fig. 11 Model simulations with additional nanoparticle potassium clearance mechanism included. Despite strong discharge of the interneuron, extracellular potassium remains close to its reference level and pyramidal cell resumes normal firing when $GABA_A$ mediated inhibition decreases due to chloride accumulation. These results illustrate that hypothetical artificial potassium clearing mechanisms could lead to effective antiepileptic treatment
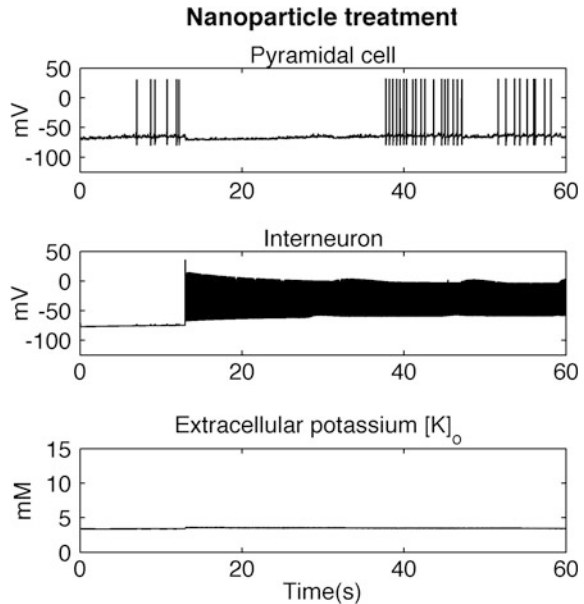
Fig. 12 Simulation results of the model with constant ionic concentrations. Strong discharge of the interneuron (*middle panel*) inhibits the pyramidal cell, which stops firing (*top panel*) while extracellular potassium concentration is stable at the initial value 3.5 mM. These results illustrate that in order to account for experimental results shown in Fig. 3a, ionic dynamics is essential
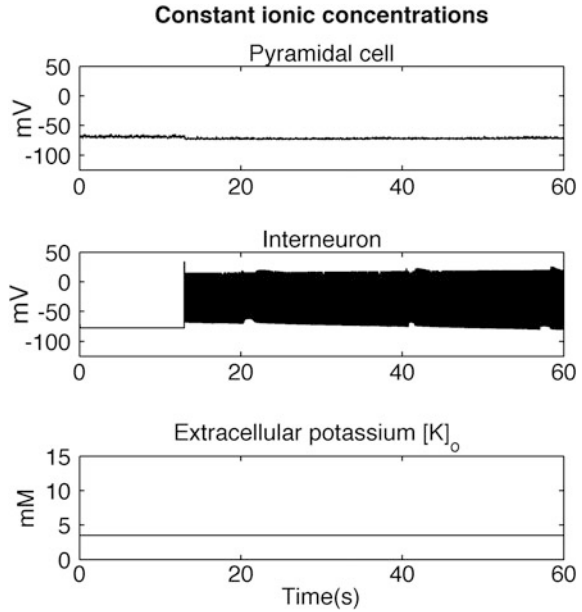
The Model with Constant Ion Concentration Gradients

In the absence of extracellular space, i.e., with constant ion concentrations, the cells communicate only through the synaptic connections and $[K^+]_o$ remains constant throughout the whole simulation and is equal to the initial value of 3.5 mM (Fig. 12, bottom trace). The inhibitory interneuron exerts strong inhibition on the pyramidal cell, which remains hyperpolarized and silent (Fig. 12, top trace). It shows that firing patterns observed experimentally and in reference simulation (Fig. 3a, b) indeed depend on activity-induced changes in intra- and extracellular ion concentrations.

"Take Home" Message for Neurologists, Psychiatrists

This computational study confirms experimentally based hypothesis that focal seizures may be triggered by strong discharges of the inhibitory interneurons. When firing-associated potassium release exceeds potassium clearance, potassium accumulates in the extracellular space, leading to generation of pathological discharges in pyramidal cells and seizure progression. This scenario challenges the traditional view of alteration in excitation/inhibition balance being the cause of epilepsy. Our study points to importance of non-synaptic mechanisms in epilepsy, especially changes in extracellular potassium. Additionally, simulations reveal the very fine

balance that exists between potassium release and uptake and identify dominant processes responsible for observed overall potassium dynamics. Insight into these mechanisms would be difficult to grasp by purely experimental observations.

We also show proof-of-concept of the feasibility of seizure control by a novel antiepileptic nanoparticle treatment. The proposed hypothetical mechanism would be able to recognize the level of extracellular potassium concentration in a surrounding medium, buffer excess of potassium if it exceeded a certain threshold and possibly release accumulated potassium back to the neuronal environment if the normal extracellular potassium level was restored by natural potassium homeostasis mechanisms. Nanoparticle therapies already exist as alternative means for drug and gene delivery and their applications towards ion absorption, like the one hypothesized here, might be possible in the future.

"Take Home" Message for Computationalists

Our modelling study, as well as some other models mentioned earlier, suggest that accurate modelling of seizure activity should include activity dependent changes in intra- and extracellular concentrations and ion homeostasis mechanisms. Significant shifts in ion concentration gradients are observed during epileptic seizures [7] and it is reasonable to assume that seizure initiation, maintenance and termination are causally related to the ionic dynamics. Our model with constant ion concentrations cannot reproduce experimental results (Fig. 12) and couldn't contribute to understanding the key mechanisms that determine seizure initiation and evolution. It shows that in order to explain pathophysiology of seizures in terms of realistic mechanisms, models should incorporate ion concentration dynamics. Such models may help to elucidate the complex interactions between neurons and their environment during seizures and may ultimately lead to development of new therapeutic strategies targeting regulation of ion concentration gradients.

References

1. Duncan JS, Sander JW, Sisodiya SM, Walker MC. 2006. Adult epilepsy. Lancet 367 (9516):1087–100.
2. Téllez-Zenteno JF, Hernández Ronquillo L, Moien-Afshari F, Wiebe S. Surgical outcomes in lesional and non-lesional epilepsy: A systematic review and meta-analysis. *Epilepsy Research* 89.2 (2010): 310–318.
3. Boon P, Vonck K, De Reuck J, Caemaert J. Vagus nerve stimulation for refractory epilepsy. Seizure 2001;10:448–455.
4. Fisher, Robert, et al. "Electrical stimulation of the anterior nucleus of thalamus for treatment of refractory epilepsy." *Epilepsia* 51.5 (2010): 899–908.
5. Lytton B. Computer modelling of epilepsy. Nat Rev Neurosci. 2008;9(8):626–37.
6. Hodgkin AL, Huxley AF. A quantitative description of membrane current and its application to conduction and excitation in nerve. J Physiol. 1952;117(4):500–44.

7. Raimondo JV, Burman RJ, Katz AA, Akerman CJ. Ion dynamics during seizures. Front Cell Neurosci. 2015, 21;9:419.

8. Fröhlich, F., Bazhenov, M., Iragui-Madoz, V., and Sejnowski, T. J. (2008). Potassium dynamics in the epileptic cortex: new insights on an old topic. Neuroscientist 14, 422–433. doi:10.1177/1073858408317955.

9. Fertziger, A. P., and Ranck, J. B. Potassium accumulation in interstitial space during epileptiform seizures. Exp. Neurol. 1970, 26, 571–585. doi:10.1016/0014-4886(70)90150-0.

10. D.M. Durand and E.H. Park, Role of potassium lateral diffusion in non-synaptic epilepsy: a com- putational study. J. of Theoretical Biology 238 (2005) 666–682.

11. H. Kager, W.J. Wadman and G.G. Somjen, Computer simulations of neuron-glia interactions mediated by ion flux. J. Comput. Neurosci. 25 (2008) 349–365.

12. Krishnan, G. P., and Bazhenov, M. Ionic dynamics mediate spontaneous termination of seizures and postictal depression state. J. Neurosci., 2011, 31;8870–8882.

13. Y. Wei, G. Ullah, and S.J. Steven, Unification of Neuronal Spikes, Seizures, and Spreading Depression. J. Neurosci. 34(35) (2014) 11733–11743.

14. M. de Curtis and V. Gnatkovsky, Reevaluating the mechanisms of focal ictogenesis: the role of low-voltage fast activity. Epilepsia 50(12) (2009) 2514–2525.

15. Johnston D and Wu SM, Foundations of Cellular Neurophysiology, MIT Press, 1995.

16. Somjen G.G. Ions in the brain: normal function, seizures, and stroke. Oxford UP, New York (2004)

17. J.A. Payne, C. Rivera, J. Voipio and K. Kaila, Cation-chloride co-transporters in neuronal com- munication, development and trauma. *TRENDS in Neurosciences* Vol. 26 No.4 (2003).

18. Peter Blaesse, Matti S. Airaksinen, Claudio Rivera, and Kai Kaila. Cation-Chloride Cotransporters and Neuronal Function. Neuron 61, 820–838, 2009.

19. Cohen, I., Navarro, V., Clemenceau, S., Baulac, M. & Miles, R. On the origin of interictal activity in human temporal lobe epilepsy in vitro. Science 298, 1418–1421 (2002).

20. M. de Curtis, A. Manfridi and G. Biella. Activity-dependent pH shifts and periodic recurrence of spontaneous interictal spikes in a model of focal epileptogenesis. J Neurosci. 18(18) (1998) 7543–51.

21. Laura Uva, Laura Librizzi, Fabrice Wendling, and Marco de Curtis. Propagation Dynamics of Epileptiform Activity Acutely Induced by Bicuculline in the Hippocampal–Parahippocampal Region of the Isolated Guinea Pig Brain. *Epilepsia,* 46(12):1914–1925, 2005.

22. Gentiletti D, Gnatkovsky V, de Curtis M, Suffczynski P. Changes of Ionic Concentrations During Seizure Transitions – a Modelling Study. IJNS (2017), in press.

23. E. Fransén, A.A. Alonso, and E.H. Michael, Simulations of the role of the muscarinic-activated calcium-sensitive nonspecific cation current INCM in entorhinal neuronal activity during delayed matching tasks. J. Neurosci. 22(3) (2002) 1081–1097.

24. Gnatkovsky V, Librizzi L, Trombin F, de Curtis M. Fast activity at seizure onset is mediated by inhibitory circuits in the entorhinal cortex in vitro. Ann Neurol 2008, 64:674–686.

25. J. Voipio, M. Pasternack, B. Rydqvist B and K. Kaila, Effect of Gamma-Aminobutyric- Acid on Intracellular pH in the Crayfish Stretch-Receptor Neuron. J. Exp. Biol. 156 (1991) 349–361.

26. Doyon N, Prescott SA, Castonguay A, Godin AG, Kröger H, De Koninck Y (2011) Efficacy of Synaptic Inhibition Depends on Multiple, Dynamically Interacting Mechanisms Implicated in Chloride Homeostasis. PLoS Comput Biol 7(9): e1002149. doi:10.1371/journal.pcbi. 1002149.

27. Kager H., Wadman W.J. and Somjen G.G., Simulated seizures and spreading depression in a neuron model incorporating interstitial space and ion concen- trations. J. Neurophysiol. 84(1) (2000) 495–512

28. Mohanraj R, Brodie MJ. (2005) Outcomes in newly diagnosed localization-related epilepsies. Seizure 14:318–323.
29. Löscher, W., Schmidt, D. Modern antiepileptic drug development has failed to deliver: ways out of the current dilemma. Epilepsia 2011;52(4):657–78.
30. Nuria Sanvicens and M. Pilar Marco. Multifunctional nanoparticles – properties and prospects for their use in human medicine. Trends in Biotechnology Vol.26 No. 8, 425–433, 2008.